

# Finite Element Modeling of Drilling Processes with Solid and Indexable Tooling in Metals and Stack-ups

T. D. Marusich, S. Usui, J. Ma and D. A. Stephenson  
Third Wave Systems, Inc  
Minneapolis, MN USA  
A. Shih  
University of Michigan  
Ann Arbor, MI USA

## Abstract

Automotive drilling operations generally entail threaded fasteners loaded in tension in steel and cast iron workpiece materials, while aerospace applications focus on holes for rivets loaded in shear in aluminum, titanium and composite stack-ups. Optimal chip flow and tool life are often in competition with burr formation, general hole quality and cycle time. Physics-based modeling of drilling processes can provide insight and information not readily available or easily obtained from experiments, and in a much faster time frame. A three-dimensional finite element-based model of drilling is presented which includes fully adaptive unstructured meshing, tight thermo-mechanical coupling, deformable tool-chip-workpiece contact, interfacial heat transfer across the tool-chip boundary, and constitutive models appropriate for high strain-rate, large strain and high temperature deformation. Explicit modeling of entrance, steady-state and exit modeling of aluminum and titanium materials, as well as metal stack-ups is performed. Drilling through stack-up layers is also shown. The modeling includes both solid twist and indexable drills. Metal cutting tests are performed and comparison with predicted data is provided.

## 1 INTRODUCTION

In order to improve metal cutting processes, i.e. lower part cost, it is necessary to model metal cutting processes at a system level. A necessary requirement of such is the ability to model interactions at the tool-chip interface and thus, predict cutter performance. Many approaches such as empirical, mechanistic, analytical and numerical have been proposed. Some level of testing for model development, either material, machining, or both is required for all. However, the ability to model cutting tool performance with a minimum amount of testing is of great value, reducing costly process and tooling iterations. In this paper, a validated finite element-based machining model is presented and employed to calculate chip geometry, cutting forces, and effects in work-hardened workpiece surface layers.

Typical approaches for numerical modeling of metal cutting are Lagrangian and Eulerian techniques. Lagrangian techniques, the tracking of discrete material points, have been applied to metal cutting [1-5]. Techniques typically used a predetermined line of

separation at the tool tip, propagating a fictitious crack ahead the tool. This method precludes the resolution of the cutting edge radius and accurate resolution of the secondary shear zone due to severe mesh distortion. To alleviate element distortions, others used adaptive remeshing techniques to resolve the cutting edge radius [3,6]. Eulerian approaches, tracking volumes rather than material particles, did not have the burden of remeshing distorted meshes [7]. However, steady state free-surface tracking algorithms were necessary and relied on assumptions such as uniform chip thickness, not allowing the modeling of milling processes or segmented chip formation .

In this paper, a three-dimensional Lagrangian finite element-based machining model is applied in to nose turning process in AISI4340. Techniques such as adaptive remeshing, explicit dynamics and tightly coupled transient thermal analysis are integrated to model the complex interactions of the cutting tool and workpiece.

Simulations were performed with Third Wave Systems **AdvantEdge** finite element based modeling software, which integrates advanced finite element numerics and material modeling for customize for machining applications.

## 2.1 FINITE ELEMENT NUMERICS

Third Wave AdvantEdge is an explicit dynamic, thermo-mechanically coupled finite element modeling package specialized for metal cutting. Features necessary to model metal cutting accurately include adaptive remeshing capabilities for resolution of multiple length scales such as cutting edge radius, secondary shear zone and chip load; multiple body deformable contact for tool-workpiece interaction, and transient thermal analysis.

The finite deformation kinematic and stress update formulations can be found in Marusich and Ortiz [6]. They are reviewed here in brevity. The balance of linear momentum is written as

$$\sigma_{ij,j} + \rho b_i = \rho \ddot{u}_i$$

The weak form of the principal of virtual work becomes

$$\int_B v_i \sigma_{ij,j} + v_i \rho b_i dV = \int_B \rho v_i \ddot{u}_i dV$$

Integration by parts and rearranging terms provides

$$\int_B \rho v_i \ddot{u}_i dV + \int_B v_{i,j} \sigma_{ij} dV = \int_{\partial B} v_i \sigma_{ij} n_j d\Omega + \int_B v_i \rho b_i dV$$

which can be interpreted as

(Inertial Terms) + (Internal Forces) = (External Forces) + (Body Forces)

Finite element discretization provides

$$\int_B \rho N_a N_b \ddot{u}_{ib} dV + \int_B N_{a,j} \sigma_{ij} dV = \int_{\partial B} N_a \tau_i d\Omega + \int_B \rho N_a b_i dV \quad Q_a = \int_{Bt} s N_a dV + \int_{B\tau q} h N_a dS$$

In matrix form

$$\mathbf{M} \mathbf{a}_{n+1} + \mathbf{R}_{n+1}^{\text{int}} = \mathbf{R}_{n+1}^{\text{ext}}$$

where

$$M_{ab} = \int_{B0} \rho_0 N_a N_b dV_o$$

is the mass matrix

$$R_{ia}^{\text{ext}} = \int_{B0} b_i N_a dV_o + \int_{\partial B0} \tau_i N_a d\Omega_o$$

is the external force array and

$$R_{ia}^{\text{int}} = \int_{B0} P_{ij} N_{a,j} dV_o$$

is the internal force array. In the above expressions,  $N_a$ ,  $a=1, \dots, \text{numnp}$  are the shape functions, repeated indices imply summation, and a comma (,) represents partial differentiation with respect to the

corresponding spatial coordinate, and  $P_{ij}$  is the first Piola-Kirchhoff stress tensor, analogous to the engineering or nominal stress.

Thermal Equations

Heat generation and transfer are handled via the second law of thermodynamics. A discretized weak form of the first law is given by

$$\mathbf{C} \dot{\mathbf{T}}_{n+1} + \mathbf{K} \mathbf{T}_{n+1} = \mathbf{Q}_{n+1}$$

A lumped capacitance matrix  $\mathbf{C}$  is used to eliminate the need for any equation solving.

$$\mathbf{C} \dot{\mathbf{T}} + \mathbf{K} \mathbf{T} = \mathbf{Q}$$

where  $\mathbf{T}$  is the array of nodal temperatures,

$$C_{ab} = \int_{Bt} c \rho N_a N_b dV_o$$

is the heat capacity matrix,

$$K_{ab} = \int_{B0} D_{ij} N_{a,i} N_{b,j} dV$$

is the conductivity matrix, and

$$Q_a = \int_{Bt} s N_a dV + \int_{B\tau q} h N_a dS$$

is the heat source array with  $h$ , having the appropriate value for the chip or tool.

In machining applications, the main sources of heat are plastic deformation in the bulk and frictional sliding at the tool-workpiece interface. The rate of heat supply due to the first is estimated as

$$s = \beta \dot{W}^p$$

where  $\dot{W}^p$  is the plastic power per unit deformed volume and the Taylor-Quinney coefficient  $\beta$  is of the order of 0.9. The rate at which heat is generated at the frictional contact, on the other hand is

$$h = -\mathbf{t} \cdot \|\mathbf{v}\|$$

where  $\mathbf{t}$  is the contact traction and  $\|\mathbf{v}\|$  is the jump in velocity across the contact.

## 2.2 CONSTITUTIVE MODEL AND MATERIAL CHARACTERIZATION

In order to model chip formation, constitutive modeling for metal cutting requires determination of material properties at high strain rates, large strains, and short heating times and is quintessential for prediction of segmented chips due to shear-localization (Sandstrom and Hodowany 1998; Childs, 1998). Specific details of the constitutive model used are outlined in Marusich and Ortiz (1995). The model contains deformation hardening, thermal softening and rate sensitivity tightly coupled with a transient heat conduction analysis appropriate for finite deformations.

In a typical high-speed machining event, very high strain rates in excess of  $10^5 s^{-1}$  may be attained within the primary and secondary shear zones. The increase in flow stress is due to strain rate sensitivity is accounted for with the relation

$$\left(1 + \frac{\dot{\varepsilon}^p}{\varepsilon_0^p}\right) = \left(\frac{\bar{\sigma}}{g(\varepsilon^p)}\right)^{m_1}$$

where  $\bar{\sigma}$  is the effective Mises stress,  $g$  the flow stress,  $\varepsilon^p$  the accumulated plastic strain,  $\varepsilon_0^p$  a reference plastic strain rate, and  $m_1$  is the strain rate sensitivity exponent

A power hardening law model is adopted with thermal softening. This gives

$$g = \sigma_0 \Theta(T) \left(1 + \frac{\varepsilon^p}{\varepsilon_0^p}\right)^{1/n}$$

where  $n$  is the hardening exponent,  $T$  the current temperature, and  $\sigma_0$  is the initial yield stress at the reference temperature  $T_0$ ,  $\varepsilon_0^p$  the reference plastic strain, and  $\Theta(T)$  is a thermal softening factor ranging from 1 at room temperature to 0 at melt and having the appropriate variation in between.

## 2.3 CONTACT

Machining involves contact between the cutting tool and workpiece during chip formation and rubbing on relief surfaces of the workpiece. Additionally, chip-workpiece contact occurs when the chip curls over and touches the workpiece, while chip-chip contact can take place during chip segmentation. A robust and general contact algorithm is necessary to detect and correct all of the scenarios. An explicit predictor-corrector deformable contact algorithm is used. A search to detect node-on-face contact provides mesh interpenetrations during the time step. During part of the time step one surface acts as the master (rigid) and the other the slave (deformable). Interpenetrations of slave nodes are updated via computation of restoring forces during the time step. During the remainder of the time step master and slave surfaces are swapped, restoring forces computed and kinematic compatibility is achieved.

## 2.4 ADAPTIVE MESHING

Lagrangian FEM formulations involving finite deformations inherently involve mesh distortion since nodal positions track material points. Mesh distortion can cause deleterious numerical performance such as loss of accuracy, reduction of convergence rates and critical time steps, volumetric locking and element failure via inversion. Additionally, it is highly advantageous to provide mesh gradation where large variations in geometric scales (cutting edge radius and feed) and material instabilities (adiabatic shear localization) occur and need to be resolved.

Adaptive meshing techniques are the tool used to overcome such technical barriers in

Lagrangian codes. Mesh refinement is effected by element subdivision along the edges of tetrahedron, creating two smaller tetrahedra. The converse operation of mesh coarsening is performed by collapsing the edge or face of shared elements, creating fewer larger elements. Mesh improvement, ie the improvement of an aspect ratio measure, is realized through techniques comprised of edge and face swapping and nodal Laplacian smoothing.

In order to resolve the critical length scales necessary in the secondary shear zone and the inherent large deformations while maintaining computationally accurate finite element configurations, adaptive remeshing techniques are critical. Near the cutting edge radius, the workpiece material is allowed to flow around the edge radius, providing the most realistic representation of the process.

During the machining simulation, mesh health diagnostics are monitored to ensure regular element configurations are maintained, along with resolution of operative geometric (e.g., cutting edge radius) and material (e.g., adiabatic shear localizations) length scales. When mesh quality or size diagnostics are violated, adaptive meshing is triggered. Local element refinement, coarsening and gradation is performed. State variables at the nodal and integration points are mapped from the old mesh to the new mesh and the time stepping analysis proceeds.

### 3.1 DRILLING MODEL

Accuracy of finite element models for metal cutting is dependent upon a number of factors. The principal ones can be identified as material modeling and characterization, numerical formulations and process modeling approximations. Material modeling would pertain to the selection of an appropriate constitutive representation for the material. Material modeling and characterization would relate to selection of the corresponding materials tests and the correct interpretation of the data to fit the model.

Numerical formulations address the selection of such aspects as Lagrangian and Eulerian formulations, finite element formulations for incompressibility, element order, adaptive meshing techniques, resolution of length scales, thermo-mechanical coupling and so on.

The process model selected herein is a three-dimensional representation of drilling. The cutting tool geometry is prescribed for both two flute twist drills and indexable drills. Cutting tool geometries can be modeled via parametric definition, STL or STEP file import. The parametric definition for the cutting tool is shown schematically in Figure 1, with the parameters defined in Table 1.

The cutting tool is positioned relative to the workpiece according to the process parameters such as speed and feed. Modeling of the entrance of the drill into the workpiece is a transient analysis until the drill point is completely immersed into the workpiece. Often it is desirable to model the steady state conditions during drilling. This can take dozens of revolutions to model and can be computationally prohibitive. To overcome these problems an initial starting depth of the drill is allowed to be prescribed, Figure 2. The workpiece is created to accurately represent the walls of the hole as well as the bottom surface of the hole created at that point. This is performed through a series of detailed boolean operations between the tool and workpiece. This allows immediate engagement of the drill and workpiece and dramatically speeds up the computational analysis. The analogs for indexable drilling are shown in Table 2, Figure 3 and Figure 4

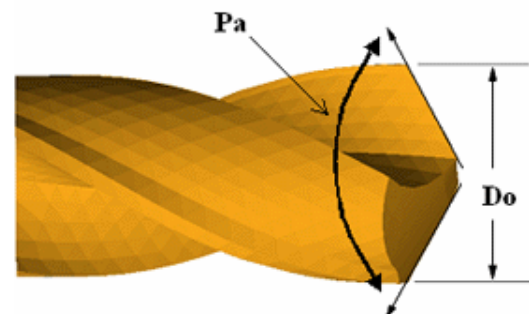


**Figure 1.** Parameterization of a two fluted twist drill is shown with design parameters.

An example of the initial set up for a twist drill simulation is shown in Figure 5. The drill simulation is shown to start at a fixed depth beneath the surface where the entire drill point is engaged with the workpiece. The final mesh with temperatures and chip formation are shown in Figure 6. The model is able to handle the complicated contact and meshing considerations required for twist drill modeling with a fully engaged tool.

The next analysis contains a multi-material stack-up with a pilot hole for an indexable drill, Figure 7. The model is focused on the area where the drill cuts through the interfacial layer, so a starting depth is applied. Chip formation is shown Figure 8. The chip formation includes cutting both materials simultaneously.

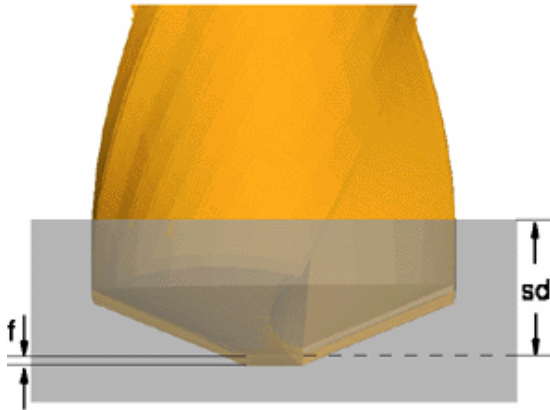


**Figure 2.** Starting point for two flute twist drill within the workpiece. “sd” is the starting depth of the tool within the workpiece with the feed, f, shown.

**Table 1 Parameters for Twist Drill**

Parameter	Name
Do	Drill Diameter
Ha	Helix Angle
w	Web Thickness
Fl	Flute Length

**Table 2 Parameters for Indexable Drill**

Parameter	Name
Shape	ISO Designation
Ld	Inscribed Diameter
R	Corner Radius
T	Insert Thickness
Ca	Clearance Angle
R	Edge Radius
D	Drill Diameter
Ha	Helix Angle

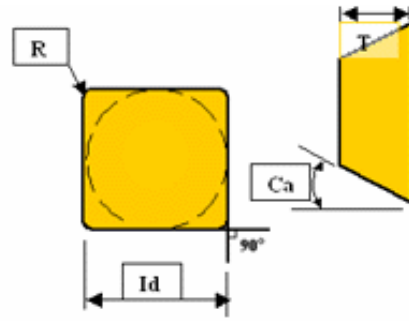


**Figure 3.** Parameters for indexable drill are shown.

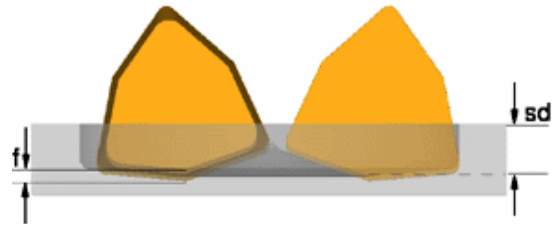


**Figure 4.** Cutting tool and workpiece positioning showing feed and depth of cut (DOC) directions.

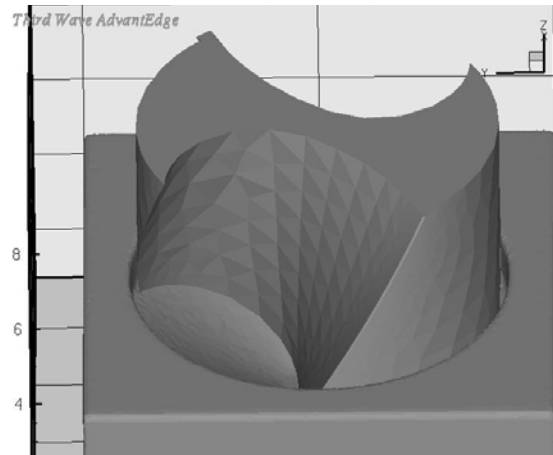


**Figure 5.** The initial mesh for the twist drill simulation is shown with an initial starting depth.

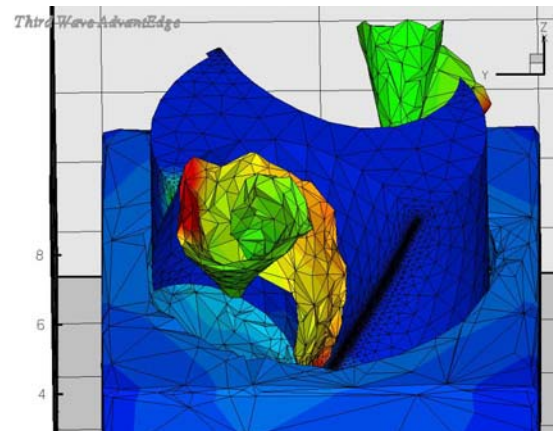


**Figure 6.** The final chip formation for the twist drill simulation is shown. The finite element mesh is overlaid on the drill, workpiece and chips. Contours of

temperature are shown, depicting heat generation and flow during the hole-making process.

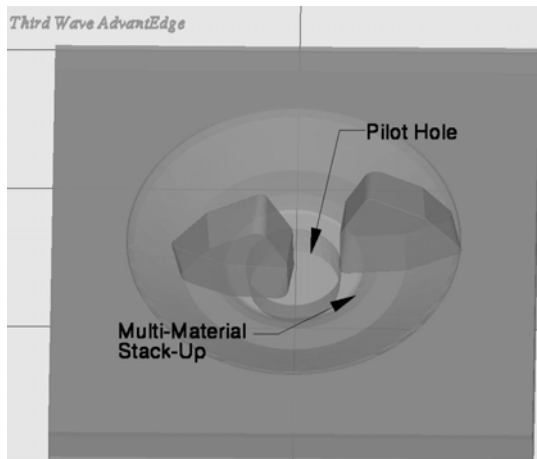


**Figure 7.** The initial model set-up is shown for an indexable drilling process. In this case, a pilot hole is modeled with multiple materials stacked on top of each other. The drill model is given at an initial starting depth.

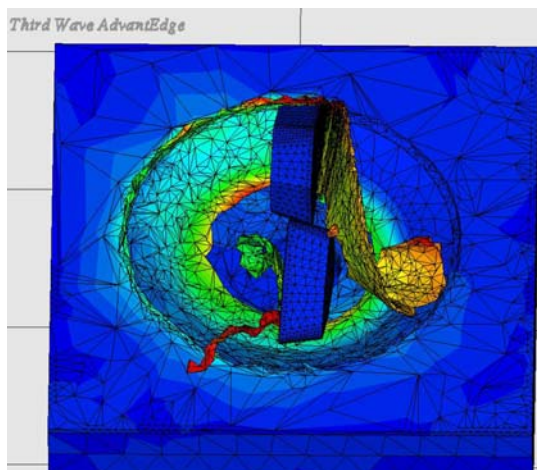


**Figure 8.** The final chip formation of the indexable drilling process with a pilot hole, initial starting depth and in a multi-material stack-up is shown. Temperature contours are shown with the finite element mesh overlaid.

#### 4. 2 FORCE VALIDATION COMPARISON

Experimental thrust force and drilling torque data was generated by University of Michigan, Figure 9 and Figure 10. The drills used were 3.97 mm in diameter and tests were performed at 0.05 mm/rev feed, and 734 rev/min and 1468 rev/min spindle speeds. AdvantEdge simulations were performed by Third Wave Systems. Simulation results were analyzed and compared with the experimental test data, Figure 11. It was observed that the model prediction for thrust force was within 15% of experimental thrust force at 734 rev/min speed

and within 25% at 1468 rev/min, Figure 12. Work continues on the comparison of predicted and measured forces for model validation and ongoing model improvement.

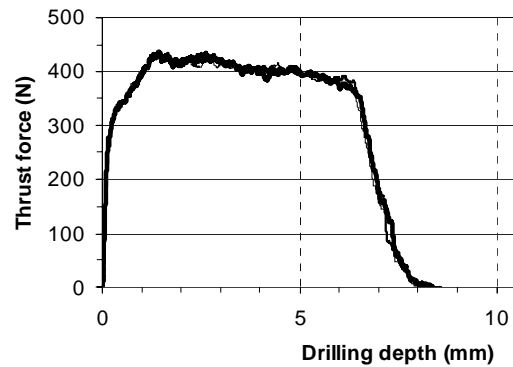


**Figure 9.** Experimental Thrust Force data from University of Michigan, for drill diameter of 3.97mm, 734 Rev/Min and 0.050 mm/rev.

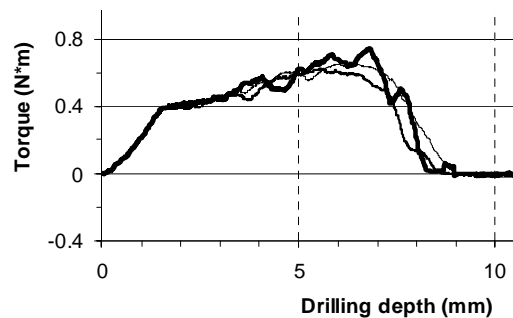


**Figure 10.** Experimental Torque data from University of Michigan, for drill diameter of 3.97mm, 734 Rev/Min and 0.050 mm/rev.

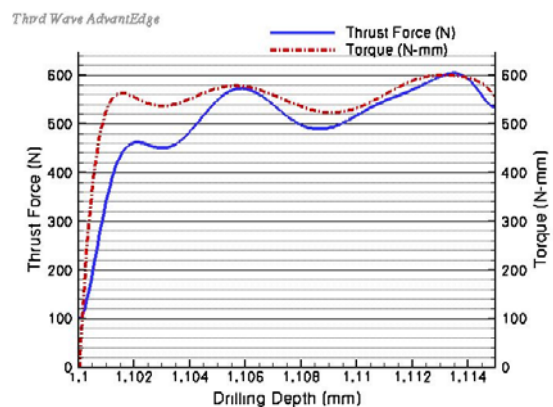


**Figure 11.** Model predicted Torque and Thrust Force.

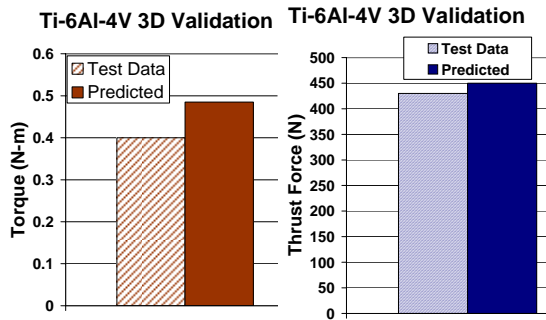


**Figure 12.** Validation Data for drilling with 3.97 mm diameter drill, 734 Rev/Min and 0.05 mm/rev feed

## CONCLUSIONS

A three-dimensional FEM model is presented which includes fully adaptive unstructured mesh generation, tight thermo-mechanically coupling, deformable tool-chip-workpiece contact, interfacial heat transfer across the tool-chip boundary, momentum effects at high speeds and constitutive models appropriate for high strain rate, finite deformation analyses. The FEM model is applied to drilling operations. Metal cutting tests are performed, cutting force components collected, and validation comparison is made. Work continues on the comparison of predicted and measured data for ongoing model validation and improvement.

## REFERENCES

1. Strenkowski, J.S. and Carroll, J.T., III, "A Finite Element Model of Orthogonal Metal Cutting," *J. Engrg. Ind.*, **107** (1985), 349-354.
2. Komvopoulos, K. and Erpenbeck, S.A., "Finite Element Modeling of Orthogonal Metal Cutting," *J. Engrg. Ind.*, **113** (1991), 253-267.
3. Sekhon, G.S. and Chenot, J.L., "Numerical Simulation of Continuous Chip Formation During Non-Steady Orthogonal Cutting," *Engineering Computations*, **10** (1993), 31-48.
4. Obikawa, T. and Usui, E., "Computational Machining of Titanium Alloy-Finite Element Modeling and a Few Results," *Journal of Manufacturing Science and Engineering*, **118** (1996).
5. Obikawa, T., Sasahara, H., Shirakashi, T. and Usui, E. "Application of Computational Machining Method to Discontinuous Chip Formation,"

*Journal of Manufacturing Science and Engineering*, **119** (1997), 667-674.

6. Marusich, T. D. and Ortiz, M., "Modeling and Simulation of High-Speed Machining", *Int. J. Num. Meth. Eng* **38** (1995), 3675-94.
7. Strenkowski, J. S. and Athavale, S. M., "A Partially Constrained Eulerian Orthogonal Cutting Model for Chip Control Tools," *Journal of Manufacturing Science*, **119** (1997), 681-688.
8. Sandstrom, D. R. and Hodowany, J. N., "Modeling the Physics of Metal Cutting in High-Speed Machining," *Machining Science and Technology*, **2** (1998), 343-353.
9. Childs, T. H. C., "Material Property Needs in Modeling Metal Machining," *CIRP Workshop on Modeling Metal Cutting*, (1998).

